The magnetic phase diagram of the itinerant-electron-type helical-spin-glass re-entrant magnet $Cr_{0.81}Mn_{0.19}Ge$

1999 J. Phys.: Condens. Matter 11 4231

(http://iopscience.iop.org/0953-8984/11/21/310)

J. Phys.: Condens. Matter **11** (1999) 4231–4249. Printed in the UK PII: S0953-8984(99)01543-X

The magnetic phase diagram of the itinerant-electron-type helical-spin-glass re-entrant magnet $Cr_{0.81}Mn_{0.19}Ge$

T Sato and K Morita

Department of Applied Physics and Physico-Informatics, Faculty of Science and Technology, Keio University, 3-14-1 Hiyoshi, Kohoku-ku, Yokohama-shi, Kanagawa 223-8522, Japan

Received 3 February 1999

Abstract. The magnetic phase diagram of an itinerant-electron-type helical-spin-glass re-entrant magnet, $Cr_{0.81}Mn_{0.19}Ge$, is determined on the basis of measurements of the alternating-current (ac) susceptibility and magnetoresistivity in transverse and longitudinal fields, which are sensitive to the magnetic response of each spin component of the modulated spin ordering. The phase boundary line is essentially the same as that of typical itinerant-electron-type helical magnets, except for the appearance of spin-glass behaviour at low temperatures. The transverse ac susceptibility provides evidence of the coexistence of modulated spin order and spin-glass behaviour in the low-temperature phase, where spin freezing appears in the transverse component of the modulated spin structure. This is consistent with the mean-field picture of the vector spin glass.

1. Introduction

The magnetic nature of itinerant-electron-type magnetic materials, including spin frustration and randomness, has rarely been studied, despite the numerous investigations of metallic spin glasses carried out during the last 25 years. The picture of Stoner glass has predicted a possible spin-glass phase produced by the interaction between weakly localized spins [1], although an experimental approach for investigating the nature of such a spin-glass phase has not yet been developed. Furthermore, knowledge of the behaviour of frustrated spins in a weakly ordered magnetic metal may yield new criteria for evaluating the appearance of the re-entrant spin glass.

Previous magnetic and neutron scattering studies by the present authors have suggested that the Mn-doped chromium monogermanide with B20-type structure, $Cr_{1-x}Mn_xGe$ with $0.17 \leqslant x \leqslant 0.21$, has a helical magnetic phase that is followed by spin-glass-like irreversible behaviour occurring at lower temperatures [2–5]. The small-angle neutron scattering (SANS) data for $Cr_{0.81}Mn_{0.19}Ge$ suggest that helical spin modulation with a very long period of $\sim$400 Å is stable at temperatures lower than $\sim$13 K in a zero magnetic field. This spin modulation changes to a ferromagnetic spin arrangement via a conical spin structure in response to a comparatively weak field of several hundred Oe. This can be interpreted as a stage of itinerant-electron magnetic behaviour, which has been observed in weakly ordered helical magnets, e.g., MnSi [6] and $Fe_xCo_{1-x}Si$ [7]. At low temperatures below $\sim$8 K, on the other hand, the following spin-glass-like characteristics have been observed: (1) thermal irreversibility of static magnetization, (2) a long relaxation of thermoremanent magnetization (TRM), (3) an anomalous peak in the temperature dependence of non-linear susceptibility, and (4) a decrease in the SANS intensity corresponding to the helical spin modulation. In addition, recent neutron

0953-8984/99/214231+19$19.50

depolarization measurements have shown that this singular behaviour can be interpreted in relation to the mean-field-type picture of spin glass [5]. Thus, the $Cr_{1-x}Mn_xGe$ system is regarded as a typical itinerant-electron-type weakly ordered magnet with spin frustration and randomness. Despite these experimental data which have been measured on various spatial and timescales, we have not been able to obtain a reliable picture of the coexistence of helical spin modulation and spin freezing.

The vector spin glass has been characterized in terms of the longitudinal and transverse order parameters which are related to the freezing of each spin component [8]. In a non-zero field, the freezing of the transverse spin component with weak irreversibility is followed by longitudinal freezing [9] as temperature decreases. Thus, it is essential to evaluate the magnetic behaviour of each spin component in order to characterize the magnetic transition of vector spin glasses. Various experimental methods have been used to separately detect the freezing behaviour of each spin component. One of the most effective and direct experimental methods for this purpose is to measure the ac susceptibility in parallel and perpendicular bias fields, i.e., the longitudinal and transverse ac susceptibilities. The other experimental method is to measure the electrical resistivity in a magnetic field applied either parallel or perpendicular to the electric current, i.e., the longitudinal and transverse magnetoresistivities. In a helical magnet, on the other hand, the spin components parallel and perpendicular to the screw axis of helical spin modulation show an anisotropic magnetic response, e.g., the difference between longitudinal and transverse magnetic susceptibilities [5]. Therefore, the above-mentioned experimental methods, which are sensitive to the magnetic response of each spin component, are necessary to characterize the mixed phase of helical ordering coexisting with spin-glass behaviour.

In the present study, we examine the characteristics relevant to the helical spin ordering and spin-glass behaviour of $Cr_{0.81}Mn_{0.19}Ge$ using the ac susceptibility and magnetoresistivity measured in the longitudinal and transverse fields. On the basis of these measurements, we first determine a conical–ferromagnetic phase boundary line and a high-temperature paramagnetic–ferromagnetic crossover line. Next, the spin-glass transition is evaluated. In addition, we specify which of the spin components correlates with the spin-freezing behaviour. Finally, we complete the magnetic phase diagram of $Cr_{0.81}Mn_{0.19}Ge$ on the basis of the present experimental data as well as information obtained in previous studies.

2. Experimental procedure

The polycrystalline $Cr_{0.81}Mn_{0.19}Ge$ sample was prepared as described in a previous study by the present authors [10]. The ac susceptibility (frequency of 210 Hz and ac field of 6 Oe) was measured by a Hartshorn-type mutual inductance bridge. A spherical sample of $\sim$3 mm in diameter was used for the magnetic measurement. The real and imaginary components of ac susceptibility can be separately measured by a lock-in amplifier, although we primarily paid attention to the in-phase response. The longitudinal ac susceptibility $\chi_{\parallel}$ and the transverse ac susceptibility $\chi_{\perp}$ were measured in a dc field applied parallel or perpendicular to the ac field using an air-core coil and an electromagnet at a field up to 450 Oe, respectively [11, 12]. The following two cooling procedures were used:

(a) The zero-field-cooling (ZFC) procedure: the sample is cooled in a zero dc field from room temperature to the desired temperature, and the desired dc field is then applied.
(b) The field-cooling (FC) procedure: the sample is cooled in the desired dc field.

The non-linear susceptibility, $3/4\chi_2^t h^2$, is also obtained by extracting the $3f$-component (f: frequency of the ac driving field) from the ac magnetic response with several values

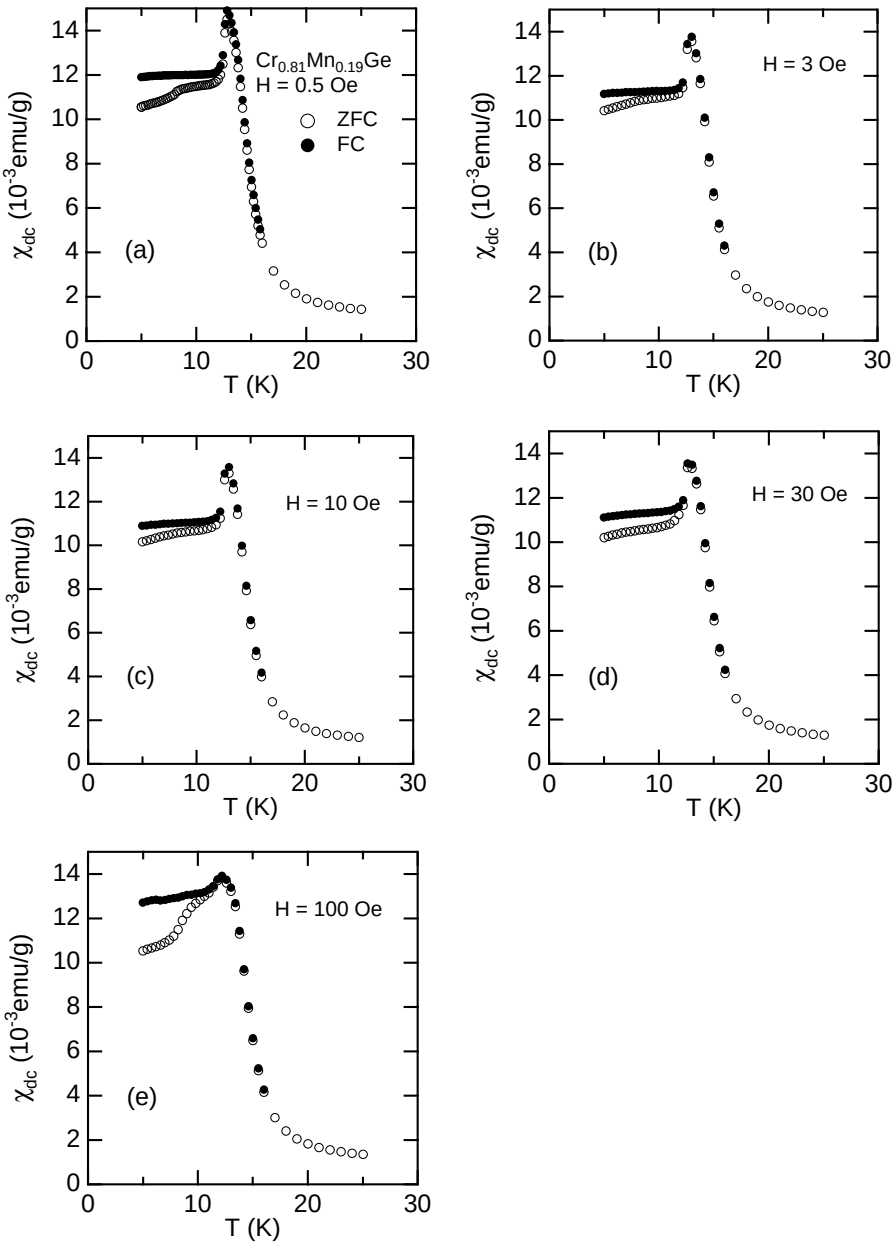

Figure 1. The temperature-dependent low-field dc susceptibility χ_{dc} of $Cr_{0.81}Mn_{0.19}Ge$ measured at various values of magnetic field below 100 Oe. The open and closed circles represent the zero-field-cooled (ZFC) and field-cooled (FC) conditions.

of frequency up to 210 Hz [13]. In addition, the low-field dc susceptibility was measured using a Quantum Design MPMS5 superconducting quantum interference device (SQUID) magnetometer.

The electrical resistivity, $\rho(H)$, was measured for a sample formed as a $10 \times 2 \times 0.8$ mm^3 plate using the ac four-terminal technique with an alternating current source (70 Hz) in a field

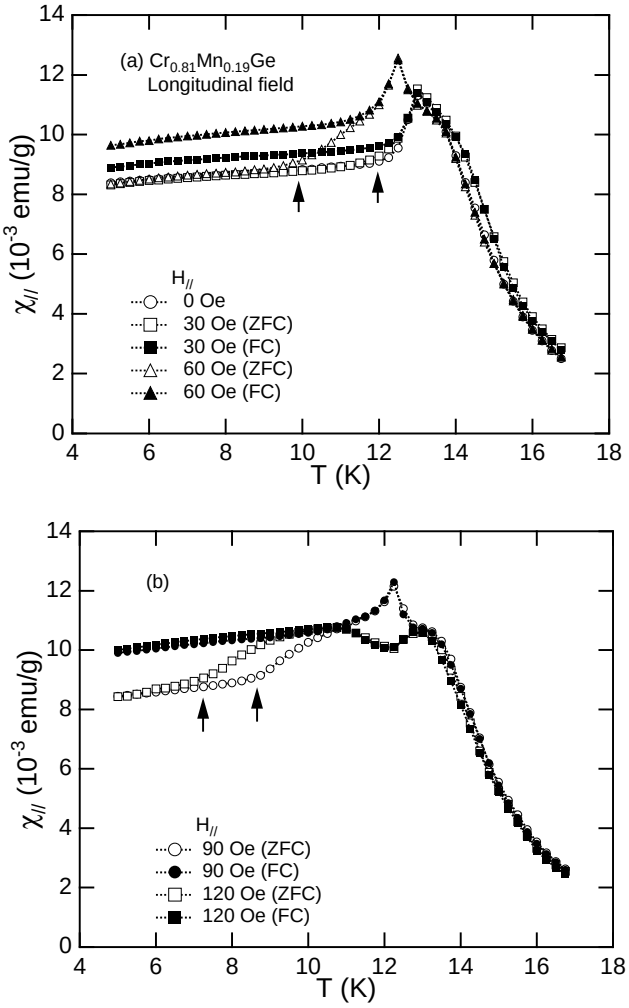

Figure 2. The temperature dependence of the longitudinal ac susceptibility $\chi_{\parallel}$ of $Cr_{0.81}Mn_{0.19}Ge$ measured at various values of dc magnetic fields at a frequency of 210 Hz. The open and closed circles represent the zero-field-cooled (ZFC) and field-cooled (FC) conditions. The arrows in (a) and (b) indicate the temperature at which the susceptibility measured at non-zero field deviates from that at zero field. The arrow in (d) shows an inflection point of the susceptibility that determines the phase boundary between the modulated spin-ordered state and the field-induced ferromagnetism.

up to 3000 Oe. The output voltage was detected using a lock-in amplifier. The longitudinal and transverse magnetoresistivities, $\Delta\rho_{\perp\parallel} = \rho_{\perp\parallel}(H) - \rho(0)$, were obtained as a function of magnetic field. In addition, the temperature dependence of $\Delta\rho$ was investigated under the FC condition.

3. Experimental results

3.1. Magnetic measurements

Figure 1 shows the temperature dependence of the low-field dc susceptibility of $Cr_{0.81}Mn_{0.19}Ge$ measured at various amplitudes of field. As mentioned in the previous paper, a hump in the

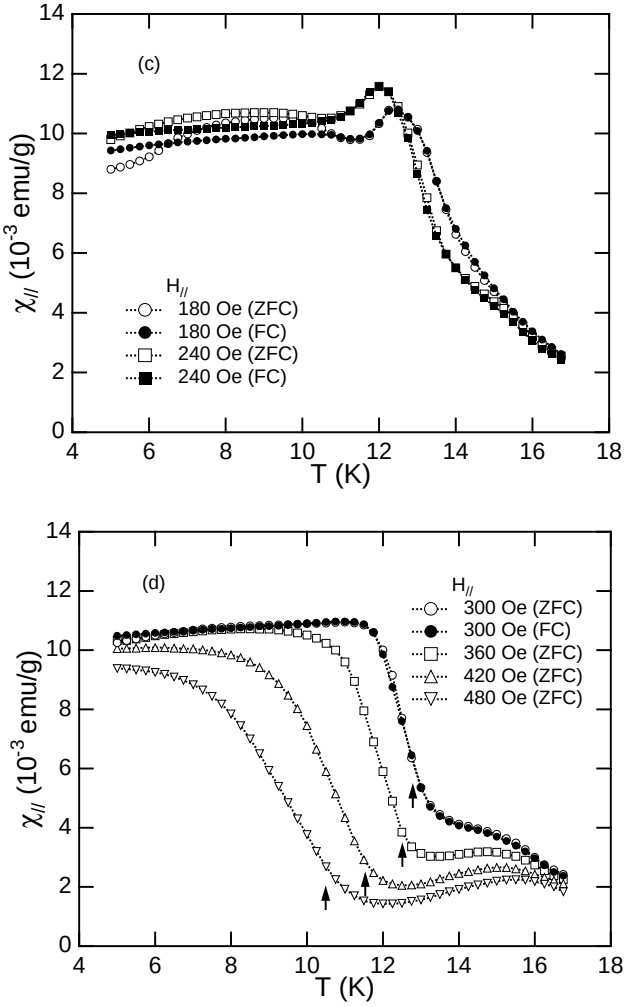

Figure 2. (Continued)

ZFC data measured at $H = 0.5$ Oe, which is related to the spin-glass transition, is observed at about 8 K in addition to a sharp maximum corresponding to the appearance of helical spin ordering ($T_c = \sim$13 K), whereas the FC data show no anomalous behaviour around 8 K. As the magnetic field increases, this hump becomes vague, and thus we lose track of the spin-glass transition. As a result, the dc magnetic susceptibility is insufficient to detect the appearance of spin-glass-like behaviour in a non-zero field. This is because the dc magnetic susceptibility only reflects the magnetic response of a spin component along an applied magnetic field.

Figure 2 shows the temperature dependence of the longitudinal ac susceptibility $\chi_{\|}$ measured at various amplitudes of dc field. Diverse characteristics appear, depending on the dc field. In the lowest-field data (figure 2(a)), the ZFC susceptibility is independent of the dc field at low temperatures, and the deviation from the $H = 0$ data appears with increases in temperature. The temperature at which the deviation occurs (arrows in figure 2(a)) decreases as the magnetic field increases. In addition, the temperature at which the irreversible behaviour begins to appear between ZFC and FC susceptibilities becomes lower as the field increases.

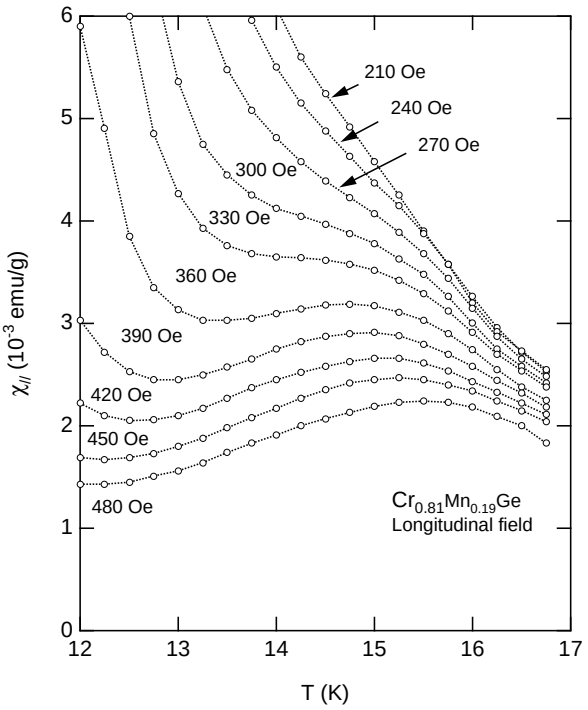

Figure 3. An expanded view of the temperature-dependent longitudinal ac susceptibility $\chi_{\parallel}$ of $Cr_{0.81}Mn_{0.19}Ge$ at temperatures around the helical transition temperature T_c, where a round peak is induced with increase in field.

Similar behaviour can be observed up to a field of 120 Oe (figure 2(b)). These characteristics reflect the low-field spin arrangement peculiar to the helical ordering in $Cr_{0.81}Mn_{0.19}Ge$, i.e., the q-vector of helical modulation is gradually arranged along an applied field as the field increases. At fields higher than 180 Oe (figure 2(c)), the ZFC susceptibility surpasses the FC data over a wide temperature range. This complicated behaviour reflects the change in spin configuration from a helical to a conical state. In the highest-field data (figure 2(d)), both the singular peak corresponding to the helical transition and the thermal irreversible behaviour can scarcely be observed. In addition, the onset temperature at which the susceptibility rapidly decreases with increases in temperature is significantly lowered with increases in the magnetic field. The inflection point in the thermal evolution of the susceptibility is represented by an arrow in figure 2(d). On the other hand, a round peak, corresponding to the crossover from the paramagnetic phase to field-induced ferromagnetism [14], appears at a temperature higher than T_c. This peak becomes pronounced, and the peak temperature slowly increases as the magnetic field increases (figure 3). These increases indicate that the ferromagnetic ordering is gradually stabilized as the magnetic field increases.

Figures 4(a)–4(d) show the temperature dependence of the transverse ac susceptibility $\chi_{\perp}$ measured at various amplitudes of magnetic field. The thermal evolution of the low-field data (figure 4(a)), measured at fields less than 120 Oe, has some features in common with those of the longitudinal susceptibility (figures 2(a) and 2(b)), except for the opposite relation between the magnitudes of the ZFC and FC susceptibilities. In order to interpret this kind of low-field behaviour, the following must be kept in mind: (1) the FC susceptibility separately

detects the magnetic responses from the longitudinal and transverse spin components of the conical structure in contrast to the isotropic response from the ZFC susceptibility and (2) the magnetic response of the longitudinal spin component exceeds that of the transverse component [5]. The intermediate-field data (figure 4(b)) reflect the change in the spin configuration from a helical to a conical state. In the highest-field data (figure 4(c)), a significant difference is observed between the longitudinal and transverse susceptibilities. First, we observe the smooth temperature dependence of $\chi_\perp$ at temperatures higher than T_c, in contrast to the longitudinal data in which the round peak is induced as the magnetic field increases. In addition, the maximum in $\chi_\perp$ remains in this region, and the temperature corresponding to the maximum decreases gradually from T_c as the magnetic field increases. Next, the thermal irreversible behaviour of $\chi_\perp$ remains even at the highest magnetic field (480 Oe), as shown in figure 4(d), which is exclusively observed in the transverse susceptibility. The temperature at which the irreversibility appears is weakly dependent on the dc field. These features observed in $\chi_\perp$ are related to the spin-freezing phenomenon, as will be discussed in the following section.

Figure 5(a) shows the temperature-dependent behaviour of the non-linear susceptibility measured at various values of frequency. A sharp negative peak appears approximately at T_c, and the peak temperature is only very weakly dependent on frequency. In contrast, the broad peak, appearing at a temperature T_{max} that is lower than T_c, is strongly dependent on frequency. The frequency dependence of T_{max} is well described in the semi-logarithmic plot shown in figure 5(b). This frequency dependence indicates that the low-temperature peak corresponds to the spin-glass transition.

3.2. Electrical measurements

Figure 6(a) shows the temperature dependence of the electrical resistivity and the magnetic contribution $\Delta\rho = \rho - \rho_{\mathrm{CrGe}}$, which is deduced on the basis of the data for CrGe [15], as shown in the inset. The value of $\Delta\rho$ shows a linear temperature dependence rather than the T^2-dependence that is observed for the typical itinerant helical magnet MnSi [16]. This difference may originate from the difference between the distributions of Mn spins for the two systems. The derivative $\mathrm{d}\,\Delta\rho/\mathrm{d}T$ shows an anomalous peak appearing approximately at 13 K (figure 6(b)), but not any features suggesting the spin-glass transition.

Figures 7(a) and 7(b) show the electrical resistivities measured in the longitudinal and transverse dc fields. A remarkable change is observed in the neighbourhood of the helical transition temperature. This kind of behaviour has also been observed for MnSi [16]. The normalized magnetoresistivities, $\Delta\rho_{\perp\parallel} = \rho_{\perp\parallel}(H) - \rho(0)$, are shown as a function of temperature in figures 8(a) and 8(b). Both the longitudinal and transverse magnetoresistivities show a sharp peak at approximately 14.2 K. At the same temperature, the spontaneous magnetization, estimated from the high-field-magnetization data, disappears, as shown in figure 5. This behaviour suggests that a temperature of 14.2 K corresponds to the appearance of the field-induced ferromagnetic phase. At low temperatures, both of the susceptibilities show a complicated field dependence, but in different ways. To emphasize these differences, we show the differences between longitudinal and transverse magnetoresistivities, $[\rho_\perp(H) - \rho_\parallel(H)]/\rho(0)$, as a function of temperature in figure 9, with the curves shown as guides for the eyes. We note that this difference becomes significant at temperatures below $\sim$8 K. This change may therefore be relevant to the spin-freezing behaviour.

Figures 10(a) and 10(b) show the magnetic field dependences of the longitudinal and transverse magnetoresistivities measured at 4.5 K. The longitudinal magnetoresistivity shows different behaviour with increases and decreases in field below 200 Oe, but the transverse magnetoresistivity is intrinsically reversible. The two magnetoresistivities show the same field

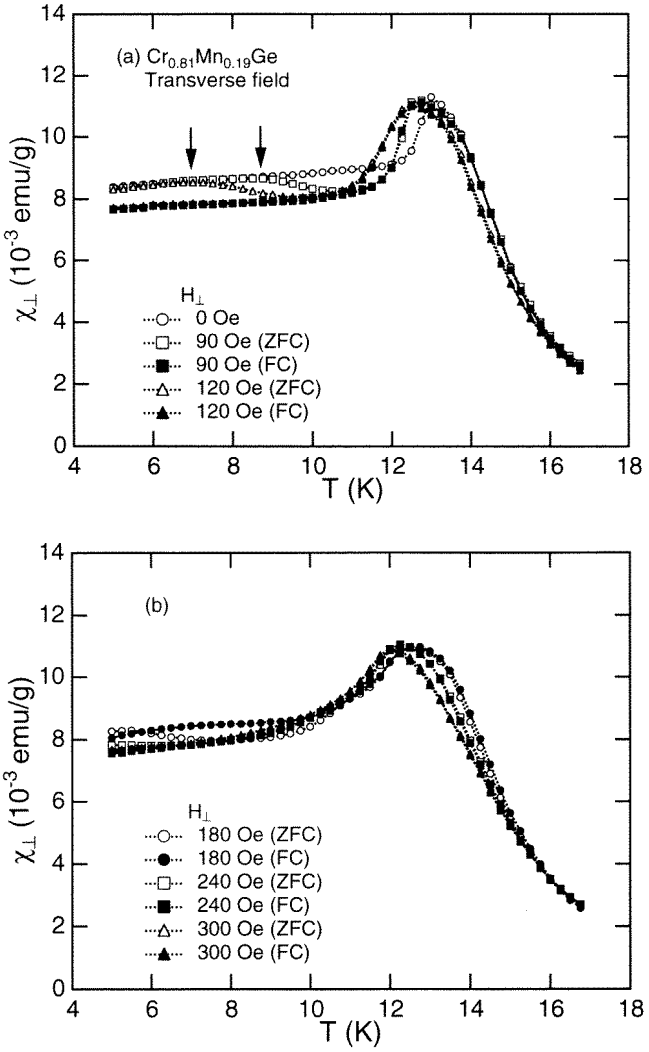

Figure 4. The temperature dependence of the transverse ac susceptibility $\chi_\perp$ of $Cr_{0.81}Mn_{0.19}Ge$ measured at various values of dc field at a frequency of 210 Hz. Open and closed circles represent the zero-field-cooled (ZFC) and field-cooled (FC) conditions. The arrow in (a) indicates the temperature at which the susceptibility measured at non-zero field deviates from the zero-field data. The arrow in (d) shows a temperature below which the thermal irreversible behaviour appears. This point corresponds to the spin-glass transition.

dependence with increases in field in the low field region. This reflects the random orientation of the q-vector of the helical spin modulation in the polycrystalline sample, as mentioned in the previous paper [2]. At a field of $\sim$200 Oe, therefore, the q-vector points in the direction of the applied field from that of the crystal axis at 4.5 K. This is consistent with the previous magnetic and neutron scattering data [2, 5]. As the magnetic field increases up to $\sim$600 Oe, each magnetoresistivity increases rapidly with a different gradient. This is well described by plotting the differences between the longitudinal and transverse magnetoresistivities (the inset of figure 10(a)). These differences become constant in the high-field region above 600 Oe.

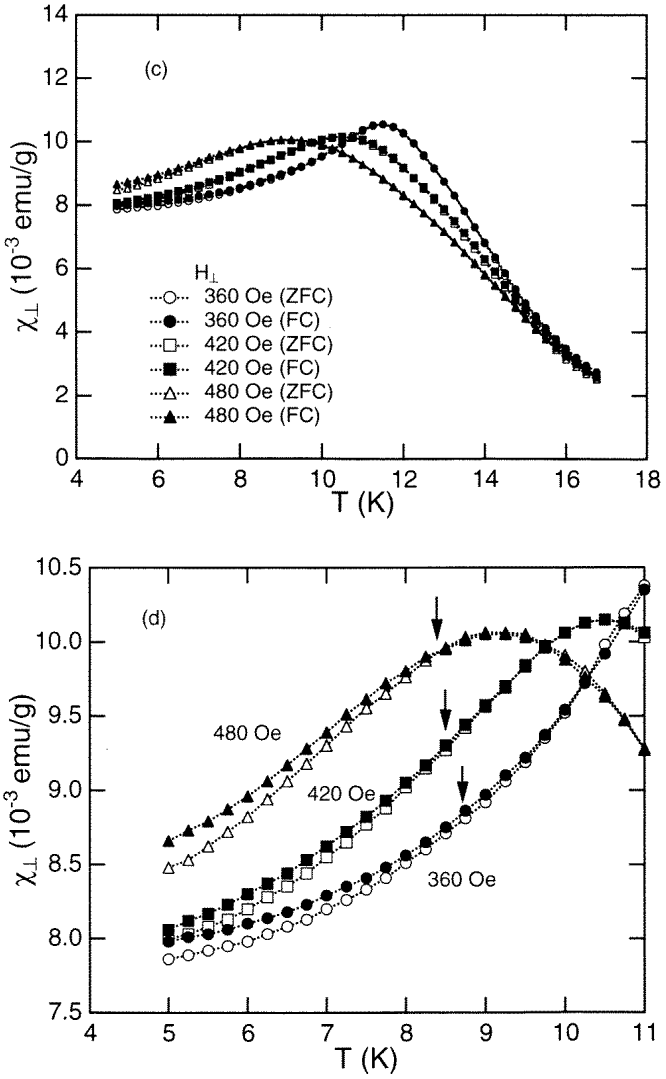

Figure 4. (Continued)

A change in the gradient appears at ∼600 Oe, which corresponds to the appearance of field-induced ferromagnetism. We should note that the transverse magnetoresistivity is larger than the longitudinal data at magnetic fields above 200 Oe. This relation is opposite to that observed for the conventional ferromagnetic material Ni [17] or spin glass NiMn [18]. We have no full explanation for this phenomenon, but it should be interpreted on the basis of the electronic structure of $Cr_{0.81}Mn_{0.19}Ge$.

4. The magnetic phase diagram

First, we abridge the characteristics relevant to the modulated spin ordering observed in the magnetic and electrical measurements. The helical transition temperature of $Cr_{0.81}Mn_{0.19}Ge$

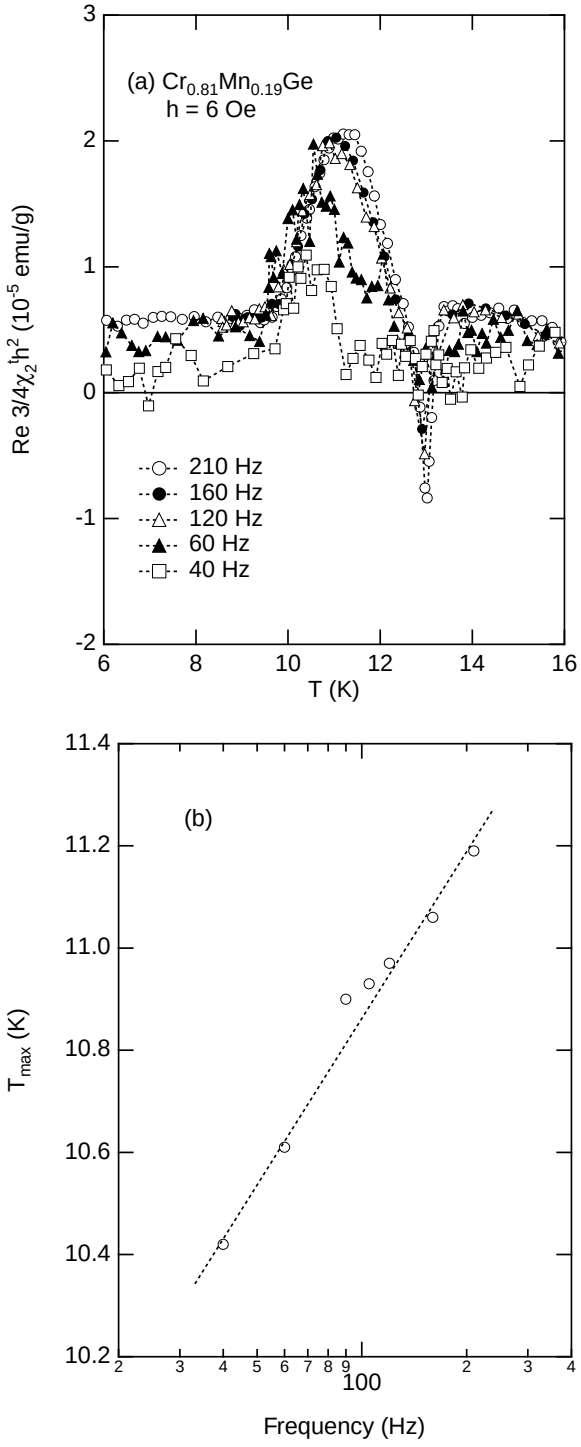

Figure 5. The temperature dependence of the non-linear susceptibility $3/4\chi_2^t h^2$ of $Cr_{0.81}Mn_{0.19}Ge$ measured at an ac field of 6 Oe at various values of the frequency (a). The maximum temperature T_{max}, corresponding to the spin-glass transition, is shown as a function of frequency in (b), where the dotted line shows the semi-logarithmic relation between T_{max} and the frequency.

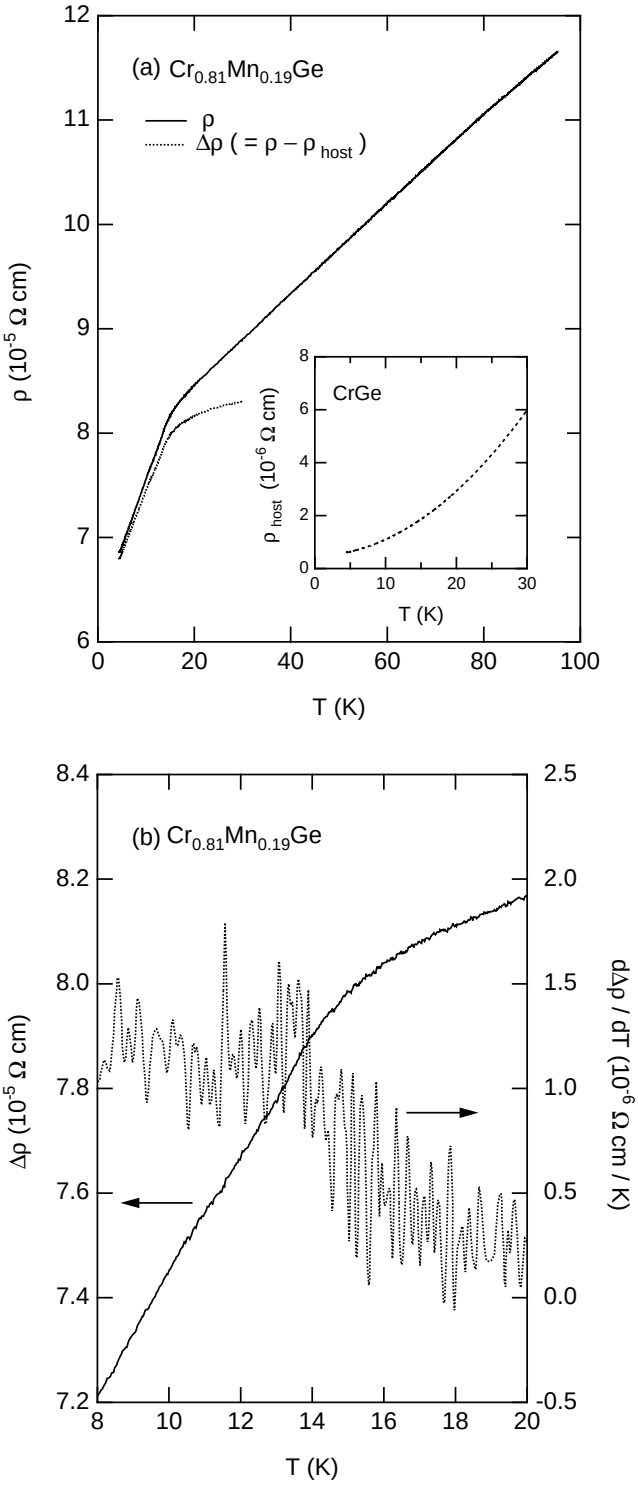

Figure 6. The electrical resistivity ρ and the magnetic contribution $\Delta\rho$ of $Cr_{0.81}Mn_{0.19}Ge$ as a function of temperature (a). The inset represents the electrical resistivity of the host material (CrGe). Expanded views of the temperature dependence of $\Delta\rho$ and its derivative are shown in (b).

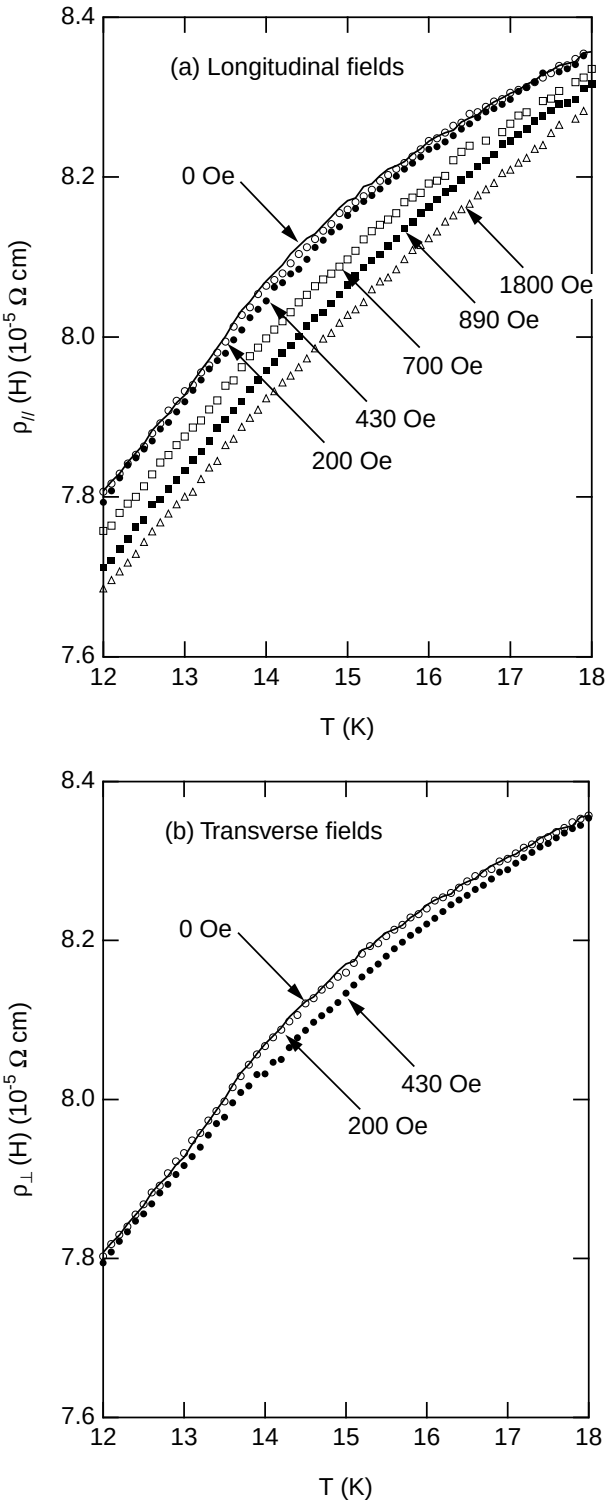

Figure 7. The electrical resistivities $\rho_{\parallel}$ and $\rho_{\perp}$ of $Cr_{0.81}Mn_{0.19}Ge$ measured in the longitudinal (a) and transverse (b) magnetic fields as functions of temperature.

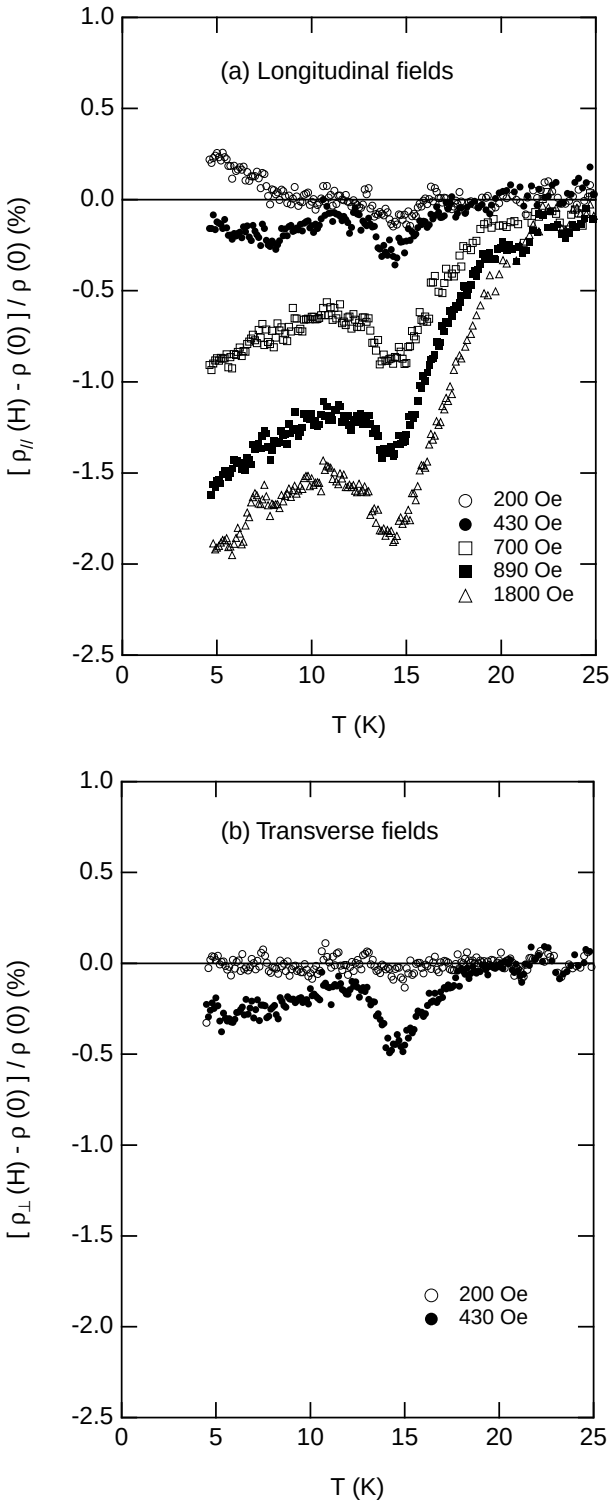

Figure 8. Normalized longitudinal (a) and transverse (b) magnetoresistivities of $Cr_{0.81}Mn_{0.19}Ge$ as functions of temperature.

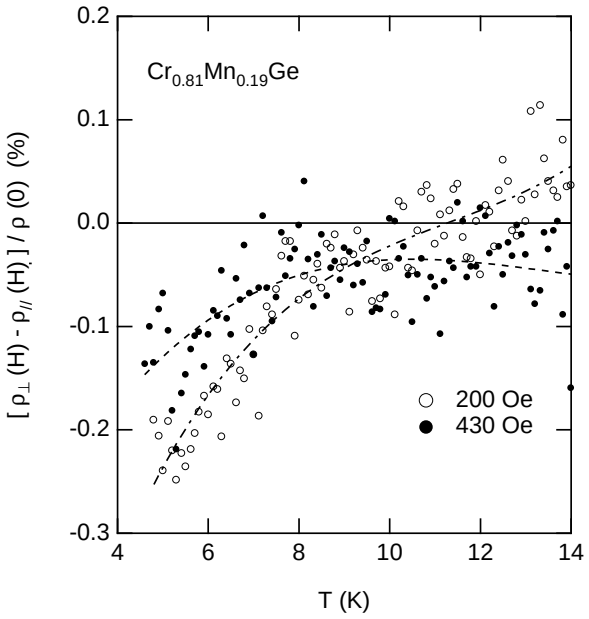

Figure 9. The difference between the longitudinal and transverse magnetoresistivities measured at fields of 200 and 430 Oe as a function of temperature.

at $H = 0$ is determined to be $T_c = 13.1$ K, on the basis of a sharp peak observed in the temperature-dependent data obtained using some experimental methods such as the low-field dc susceptibility ac susceptibility and non-linear susceptibility methods. This critical temperature is also verified by the electrical measurement, i.e., the temperature derivative of the resistivity shows a singular change at approximately 13 K. The critical temperature T_c is represented by a closed circles in the magnetic phase (H–T) diagram shown in figure 11. As mentioned, on the basis of the previous SANS experiments [2], we know that the helical spin structure changes to a conical structure as the field increases, and the transition from a conical to a ferromagnetic state occurs at a field of $H_c(T)$. In order to determine the critical field $H_c(T)$, we pay attention to the following features of the longitudinal ac susceptibility measured at temperatures higher than 300 Oe: (1) $\chi_{\|}$ weakly depends on temperature at low temperatures, although it drops rapidly as temperature increases, with the onset temperature shifting to a lower temperature as the field increases, and (2) a round peak, corresponding to the appearance of the field-induced ferromagnetic ordering, appears at a temperature higher than T_c. Feature (1) obviously corresponds to the conical–ferromagnetic transition. Therefore, we evaluate $H_c(T)$ using an inflection point in the temperature-dependent ac susceptibility measured at a field above 300 Oe (as shown by the arrows in figure 2(d)). This critical field is represented by open circles in figure 11. In addition, the magnetic field at which the magnetization becomes saturated can be regarded as $H_c(T)$ [5]. This is also plotted in the magnetic phase diagram using the symbol ◇. These individual points lie on a smooth curve. This curve is also consistent with the field-dependent spin structures evaluated on the basis of the neutron scattering data. Furthermore, we evaluated the crossover from the paramagnetic phase to the field-induced ferromagnetic phase on the basis of the round peak in the longitudinal ac-susceptibility data (feature (2)). This is represented by open triangles in figure 11. These phase boundary lines

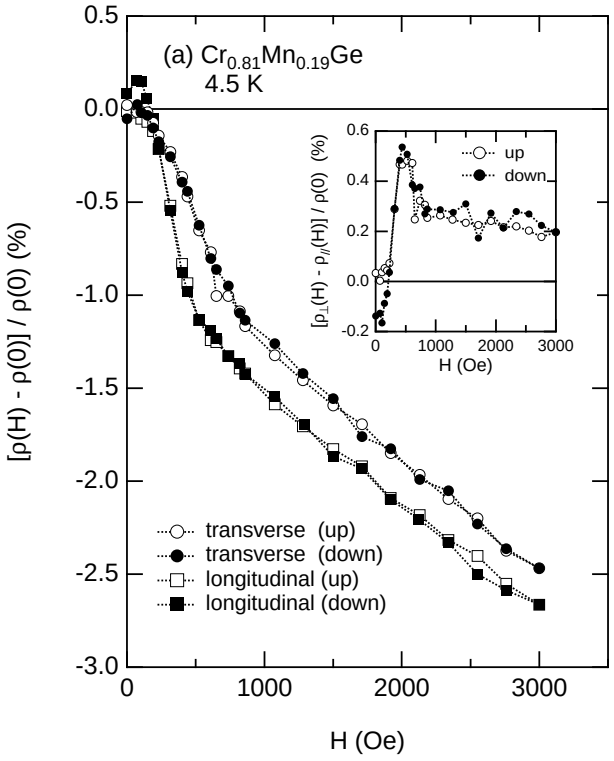

Figure 10. The field dependence of the normalized longitudinal and transverse magnetoresistivities of $Cr_{0.81}Mn_{0.19}Ge$ (a), where the open and closed symbols correspond to the data measured with increases and decreases in field, respectively. An expanded view is shown in (b). The inset shows the difference between the longitudinal and transverse magnetoresistivities as a function of magnetic field.

resemble those of the itinerant-electron-type helical magnet MnSi [14].

We next investigate the low-field spin arrangement relevant to the direction of q-vector of the spin modulation. In the polycrystalline sample, a random orientation is realized for the q-vector at $H = 0$. Thus, a change to the non-random orientation from the random state should be accompanied by a deviation in the susceptibility from the zero-field data. When the q-vector is arranged along the applied field, the ZFC susceptibility merges into the FC data measured at the same magnetic field. This type of change is observed in both the longitudinal and transverse ac susceptibilities. The onset temperature at which the deviation from the zero-field data starts to appear is plotted in the magnetic phase diagram (open squares), together with the inflection point in the magnetization curves determined previously [5] (closed squares). These data lie in almost a straight line whose extrapolate intersects the critical point $T_c(0)$. Thus, we can determine a crossover line at which the present spin system becomes free from the crystal anisotropy. This procedure enables one to separate the spin-glass phenomenon from the crossover behaviour relevant to the crystal anisotropy.

Next, we evaluate the spin-glass transition temperature $T_{sg}(H)$ as a function of magnetic field. Some traces of the spin-glass transition can be observed in the magnetic and electrical measurements: (1) a hump in the ZFC dc susceptibility measured at low magnetic field (figure 1(a)), (2) irreversible behaviour in the transverse ac susceptibility at fields higher than 360 Oe (figure 4(d)), (3) a broad maximum in the non-linear susceptibility (figure 5)

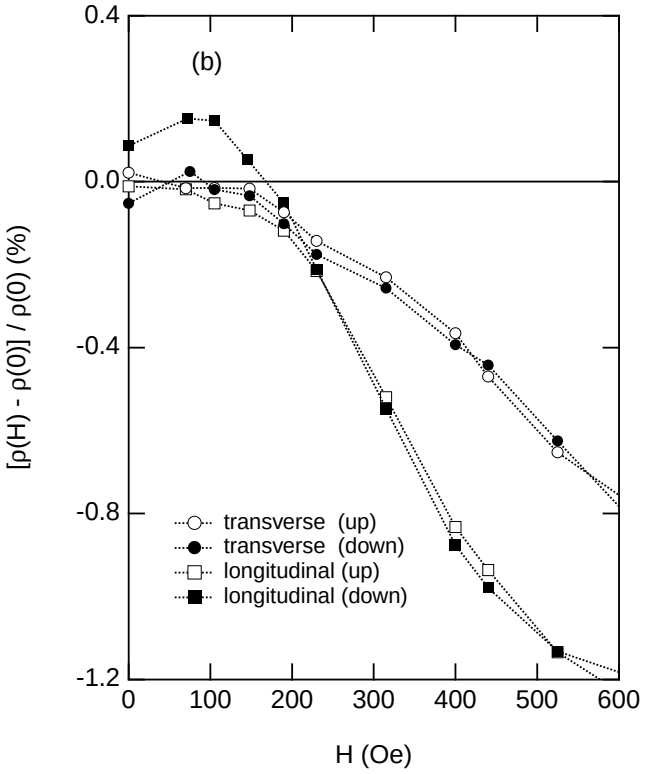

Figure 10. (Continued)

and (4) the rapid change in the difference between the longitudinal and transverse magnetoresistivities at ∼8 K (figure 8). As demonstrated in the non-linear susceptibility data (figure 5), the corresponding phenomenon is significantly dependent on the timescale of the experimental methods. Therefore, the spin-glass transition temperature should be determined by means of the static measurement, and thus we obtain $T_{sg}(0) = 8$ K on the basis of the dc susceptibility measured at the lowest magnetic field. This is represented by the symbol ▼ in the magnetic phase diagram. The value of $T_{sg}(H)$, however, cannot be determined on the basis of the dc magnetic measurement because, as shown in figure 1, the hump rapidly becomes vague with increases in the magnetic field. With the transverse ac susceptibility, on the other hand, irreversible behaviour can be observed up to the highest field (480 Oe) in the present work, although this is not true of the longitudinal ac susceptibility. It is persuasive that this type of irreversibility is related to the appearance of spin glass. Therefore, we evaluate the value of $T_{sg}(H)$ at a frequency of 210 Hz using the temperature at which the irreversibility in the transverse ac susceptibility disappears. This is represented by the symbol ▽ in the magnetic phase diagram, together with the value of $T_{sg}(0)$ at a frequency of 210 Hz, which is determined by the non-linear susceptibility. In this way, we can determine the range within which the spin-glass behaviour coexists with the helical (or conical) magnetic ordering. In addition, we should be careful to note that the spin-glass transition in a non-zero field is observed only using an experimental method that is sensitive to the magnetic response of the transverse spin component. The above indicates that spin freezing appears in the transverse component of the conical spin modulation. Finally, we note that we cannot determine whether or not the

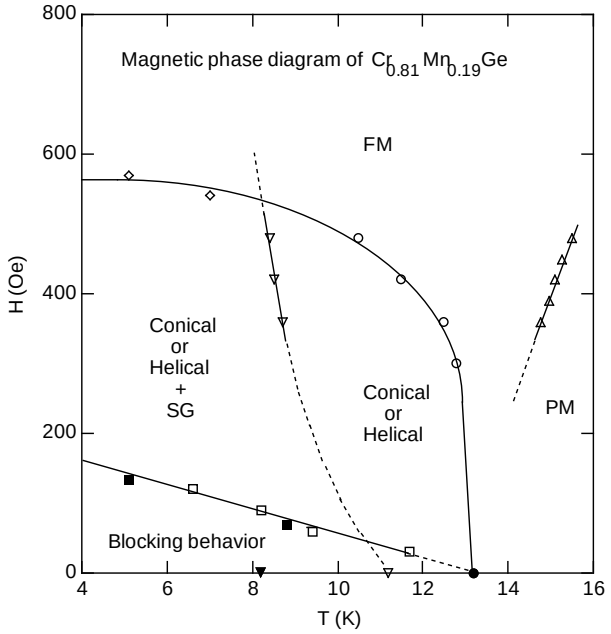

Figure 11. The magnetic phase diagram of $Cr_{0.81}Mn_{0.19}Ge$. The meanings of the symbols are explained in the text.

spin-glass phase boundary line penetrates into the field-induced ferromagnetic phase due to the narrow field range used in the present work.

5. Discussion

First, we will discuss the magnetic nature of the helical ordering in $Cr_{0.81}Mn_{0.19}Ge$. The magnetic phase boundary lines resemble to those of a typical itinerant-electron magnet MnSi, as mentioned above, i.e., the transition from the helical state to field-induced ferromagnetism via the conical spin modulation occurs at temperatures below T_c, and the paramagnetic–ferromagnetic crossover is observed above T_c. These results provide evidence that itinerant-electron-type helical spin ordering, explained in terms of the self-consistent renormalization theory [19], is realized in the present sample. This type of magnetic ordering has also been observed in other magnetic compounds with a cubic B20-type structure, such as MnSi [6] and $Fe_xCo_{1-x}Si$ [7]. This correlation supports the theoretical viewpoint that the long-period helical modulation originates from the Dzyaloshinsky–Moriya-type spin interaction, which is expected in crystal structures such as the B20-type structure that lack inversion symmetry [20, 21].

Examination of the generalized Rhodes–Wohlfarth plot [22] is also helpful in characterizing the itinerant-electron-type nature of $Cr_{0.81}Mn_{0.19}Ge$. In this plot, the value of p_{eff}/p_s is determined by a single parameter T_c/T_0 in the case of a weakly ferromagnetic limit, where p_{eff} is the effective paramagnetic moment per Mn atom deduced from the Curie–Weiss law, p_s is the magnetic moment deduced from the magnetization at 0 K and T_0 is a parameter related to the energy width of the dynamic spin fluctuation. On the basis of the previous magnetization data [5, 10], we can roughly estimate that $p_{eff}/p_s \sim 4$ and $T_c/T_0 \sim 0.05$. This pair of values

is consistent with the curve of the generalized Rhodes–Wohlfarth plot. Thus, we confirm the weakly ordered magnetic nature of the present system. In addition, we can conclude that the characteristics of the spin fluctuation in the present sample are similar to those of MnSi or $Fe_xCo_{1-x}Si$ [23]. In the electrical measurements, on the other hand, we cannot observe any feature characteristic of the itinerant-electron-type magnet. This may be because these features are hidden by the strong electron scattering resulting from the random distribution of Mn ions in the present sample.

Next, we discuss the magnetic behaviour relevant to the crystal anisotropy which is observed at low magnetic fields. The crossover behaviour, from an isotropic state in which the q-vector of spin modulation is randomly oriented to a collinear state in which the q-vector is arranged along the applied field, is observed along a line in the H–T plane. Such a crossover may be compared with the blocking phenomenon that has been observed in superparamagnetism. According to the theory of superparamagnetism [24], which provides an expression for the relaxation time of the magnetic moment over the anisotropy energy K, the crossover field is dependent on the root square of the temperature, under the condition that the anisotropy energy and magnetization are constant. In contrast, we have previously deduced the thermal evolution of K for $Cr_{0.81}Mn_{0.19}Ge$ [5], determining that there is a significant increase below $\sim$8 K. Therefore, the linear relation in the H–T plane should be interpreted on the basis of the temperature dependence of K in addition to that of the magnetization. In addition, we note that this characteristic change in K is correlated with the appearance of spin-freezing behaviour.

The spin-glass transition in $Cr_{0.81}Mn_{0.19}Ge$ can be well characterized by the transverse ac susceptibility and the difference between the longitudinal and transverse magnetoresistivities, which are sensitive to the magnetic response of a particular component of spins. On the basis of the present experiments, we conclude that spin freezing appears in the transverse spin components of conical modulation. This is consistent with the mean-field theory of vector spin glass [8] that predicts freezing in the transverse spin components with weak irreversibility that occurs prior to the spin freezing with strong irreversibility. We believe that the present data for $Cr_{0.81}Mn_{0.19}Ge$ provide reliable evidence of the transverse spin freezing in spin-glass materials. We could not obtain any evidence of spin freezing with strong irreversibility, but it may be observed at temperatures lower than those investigated in the present work. Finally, we note that the spin-freezing temperature T_{max}, defined as a round peak appearing in the non-linear susceptibility, is significantly dependent on frequency compared with the other spin-glass systems. The value of $\Delta T_{max}/[T_{max}\ \Delta(\log\omega)]$, used as an index of the frequency shift of T_{max}, is 0.13 for the present sample, which is one order larger than that of the typical spin glasses, e.g., CuMn (0.005), AuMn (0.010) and NiMn (0.018) [25]. This large frequency shift in $Cr_{0.81}Mn_{0.19}Ge$ may be related to the coexistence with the long-period spin modulation, although this cannot be discussed in detail at present.

6. Conclusions

On the basis of magnetic and electrical measurements, that are sensitive to the magnetic response of a particular spin component, we determined the magnetic phase diagram of $Cr_{0.81}Mn_{0.19}Ge$. It has typical features that have been observed for other itinerant-electron-type helical magnets: the transition from the helical state to field-induced ferromagnetism via conical spin modulation at temperatures below T_c and a paramagnetic–ferromagnetic crossover observed above T_c. In addition, we separately evaluated the spin-freezing behaviour and the blocking phenomena related to the crystal anisotropy. We confirmed the coexistence of modulated spin ordering and spin-glass behaviour at low temperatures. Furthermore, we

conclude that the spin-freezing behaviour appears in the transverse spin component of the modulated spin structure. This is consistent with the mean-field picture of vector spin glass.

Acknowledgments

The present study was supported in part by a Grant-in-Aid for Science Research from the Ministry of Education, Science and Culture. Additional support was provided by the Seki Foundation for the Promotion of Science and Technology, and by the Iketani Science and Technology Foundation.

References

[1] Hertz J A 1979 *Phys. Rev.* B **19** 4796
[2] Sato T, Ando T, Oku T and Furusaka M 1994 *Phys. Rev.* B **49** 11 864
[3] Sato T, Ando T, Oku T and Furusaka M 1995 *J. Magn. Magn. Mater.* **140–144** 1785
[4] Sato T, Taniyama T, Oku T, Ito S and Takeda M 1996 *J. Cryst. Res. Technol. Spec. Issue* 2 **31** 589
[5] Sato T, Furusaka M and Takeda M 1999 *J. Magn. Magn. Mater.* at press
[6] Ishikawa Y, Tajima K, Bloch D and Roth M 1976 *Solid State Commun.* **19** 525
[7] Beille J, Voiron J and Roth M 1993 *Solid State Commun.* **47** 399
[8] Gabay M and Toulouse G 1981 *Phys. Rev. Lett.* **47** 201
[9] de Almeida J R L and Thouless D J 1978 *J. Phys. A: Math. Gen.* **11** 983
[10] Sato T, Kozu J, Oshiden K, Nemoto T, Ohta E, Sakata M, Goto T and Sakakibara T 1988 *J. Phys. Soc. Japan* **57** 639
[11] Nemoto T, Sato T, Ohta E and Sakata M 1989 *J. Magn. Magn. Mater.* **78** 43
[12] Sato T 1990 *Phys. Rev.* B **41** 1550
[13] Ando T, Ohta E and Sato T 1996 *J. Magn. Magn. Mater.* **163** 277
[14] Kusaka S, Yamamoto K, Komatsubara T and Ishikawa Y 1976 *Solid State Commun.* **20** 925
[15] Sato T and Sakata M 1983 *J. Phys. Soc. Japan* **52** 1807
[16] Kadowaki K, Okuda K and Date M 1982 *J. Phys. Soc. Japan* **51** 2433
[17] Smith J 1951 *Physica* **17** 612
[18] Senoussi S and Öner Y 1984 *J. Appl. Phys.* **55** 1472
[19] Moriya T 1976 *Solid State Commun.* **20** 291
[20] Nakanishi O, Yanase Y, Hasegawa A and Kataoka M 1980 *Solid State Commun.* **35** 995
[21] Beck P and Jensen H M 1980 *J. Phys. C: Solid State Phys.* **13** L881
[22] Takahashi Y 1986 *J. Phys. Soc. Japan* **55** 3553
[23] Shimizu K, Maruyama H, Yamazaki H and Watanabe H 1990 *J. Phys. Soc. Japan* **59** 305
[24] Néel L 1949 *Ann. Geophys.* **5** 99
[25] Mydosh J A 1993 *Spin-Glasses* (London: Taylor and Francis) p 67